Modeling of Mid-Infrared Quantum Cascade Laser by Means of Nonequilibrium Green's Functions

Grzegorz Hałdaś, Andrzej Kolek, and Igor Tralle

***Abstract*— Nonequilibrium Green's function (NEGF) calculations of mid-infrared quantum cascade laser (QCL) that preserve real-space basis have been performed. The approach developed in this paper relies on two improvements introduced to nonequilibrium Green's functions/Poisson computational scheme. First, the boundaries of single laser stage were carefully designed as to maintain its periodicity with the whole quantum cascade structure. Second, the NEGF/Poisson solver was equipped with several controlling features that enable the restoration of convergence of the method for quite complex structures with many resonances and boundary conditions for Poisson equation set inside the structure. With this simulation tool, calculations for an anticrossed diagonal design of mid-infrared QCL have been performed. Results agree with experimental data (threshold current of ∼4.2 kA/cm^2 at material gain of ∼70/cm) and the current understanding of carrier transport in such devices.**

***Index Terms*— Nonequilibrium Green's function, quantum cascade lasers, simulation.**

I. Introduction

NON-EQUILIBRIUM Green's function approach for studying quantum transport phenomena elaborated by Keldysh [1], and Kadanoff and Baym [2] has been proved to be a powerful method of theoretical physics. The increasing capacity and speed of today's computers make this method efficient also in quantitative analysis of the "real-world" problems, an important example of which is the modeling of nanoelectronic devices. Since the pioneering work of Lake *et al.* [3] non-equilibrium Green's function (NEGF) formalism has been successfully applied to model e.g. resonant tunneling diodes [4], field effect transistors [5], carbon nanotubes [6], light-emitting diodes [7], photodetectors [8], quantum-well solar cells [9] and quantum cascade lasers (QCL) [10]–[19]. For the latter an important issue are boundary conditions applied to the simulated structure which must imitate periodicity of the real device.

In the paper the model of boundaries to be used in NEGF steady state 1D-simulator of QCL, recently proposed in [10], is further developed. The upgrade we have made preserves the following requirements: (i) charge neutrality within the laser period, (ii) translational periodicity of charge distribution, (iii) periodic repeatability of the potential $V(x)$ with the potential shift $\Delta V \equiv V(x) - V(x+\Delta) = eU = eF\Delta$, where Δ is the period length, U is the applied bias and F is the average electric field within the device. The model was applied to the QCL emitting at mid-infrared (mIR) frequencies. This structure is quite demanding as the field related to the threshold current is so strong that several ($\sim$7) phonons is emitted by the electron spanning one laser period. Then, the convergence of NEGF method slows down or even is lost. In the paper efforts were undertaken to restore the convergence and speed up the numerical procedure. Ideas from the control theory were employed, and digital controllers were used in the feedback loop of NEGF-Poisson solver to get the self-consistent solution of the equations. In the illustrative example, quantities like density of states, charge, material gain and current density in the structure of QCL were calculated for the case when electrons are scattered by the screened polar-optical phonons (pop) and interface roughness (ir).

Manuscript received December 21, 2010; revised February 16, 2011; accepted March 11, 2011. Date of current version May 9, 2011. This work was supported in part by the Polish Ministry of Science and Higher Education under Grant PBZ 10/G017/T02/2007.

G. Hałdaś and A. Kolek are with the Department of Electronics Fundamentals, Rzeszow University of Technology, Rzeszow 35-959, Poland (e-mail: ghaldas@prz.edu.pl; akoleknd@prz.edu.pl).

I. Tralle is with the Institute of Physics, University of Rzeszow, Rzeszow 35-959, Poland (e-mail: tralle@univ.rzeszow.pl).

Color versions of one or more of the figures in this paper are available online at http://ieeexplore.ieee.org.

Digital Object Identifier 10.1109/JQE.2011.2130512

II. NEGF Modeling of THz QCL

The main equations of NEGF formalism are Dyson equation for the retarded Green's function G^R and Keldysh equation for the lesser Green's function $G^<$. In general G^R and $G^<$ are the functions of energy E and two spatial coordinates **r**, **r'**. For the layered structures with translational invariance in the planes of the layers one may consider $G^{R,<}$ as functions of energy E, coordinates x, x' in the direction of transport, perpendicular to the layers, and the parameter $k_{||}$-the modulus of electron momentum in the plane of the layers [3]. Then, Dyson equation reads

$$(E - H - \Sigma^R_{scatt} - \Sigma^R_{cont})G^R = \delta(x - x'), \qquad (1)$$

where E is the energy, H device Hamiltonian and Σ^Rs are contact and scattering retarded selfenergies. Keldysh equation

$$G^< = G^R(\Sigma^<_{scatt} + \Sigma^<_{cont})G^{R*}, \qquad (2)$$

where * denotes complex conjugate, involve lesser selfenergies $\Sigma^<$. These equations are supplemented with another two which enable calculations of selfenergies Σ^R, $\Sigma^<$ with the use of G^R and $G^<$. Detailed form of these equations depend on the involved scattering mechanisms. The whole set of 4 equations is solved iteratively until self-consistent solution is achieved. Then, various quantities related to carrier transport can be

calculated. E.g. energy-spatially-momentum-resolved densities of states/electrons are directly related to G^R and $G^<$

$$N\left(E, k_{||}, x\right) = -\frac{1}{\pi}\mathrm{Im}\{G^R\left(E, k_{||}, x, x\right)\},$$

$$n\left(E, k_{||}, x\right) = \frac{2}{\pi}\mathrm{Im}\{G^<\left(E, k_{||}, x, x\right)\}.$$

Other quantities that can be calculated include current and its coherent component, scattering rates, optical absorption (gain).

The set of NEGF equations is solved in the range $0 < x < L$ which defines size of the structure (device) subjected to simulations. However, they refer to "open" device because contact selfenergies in (1) and (2) describe the effect of the leads attached to the structure at $x = 0$ (left (L) contact) and $x = L$ (right (R) contact), $\Sigma^{R,<}_{cont} = \Sigma^{R,<}_{\mathrm{L,R}}(E, k_{||})$. In the simplest case the leads are semi-infinite, scattering- and field-free homogeneous conductors in thermal equilibrium. Then, lesser contact selfenergies are related to the retarded ones as [20]

$$\Sigma^<_{\mathrm{L,R}}\left(E, k_{||}\right) = \Sigma^R_{\mathrm{L,R}}\left(E, k_{||}\right) f_{\mathrm{L,R}}\left(E, k_{||}\right), \tag{3}$$

where $f_{L,R}(E, k_{||}) = f_{L,R}(E)$ are Fermi-Dirac distributions in L and R lead. In QCL each period is surrounded by similar periods and so the energy spectrum of the carriers entering/exiting single laser period is certainly different from the spectrum of free carriers entering the structure from the homogeneous leads. Various attempts have been made in order to make the spectrum of injected/extracted carriers more realistic. Kubis *et al.* [10], [11] included scattering in the leads and attached a small portion of them to the simulated structure. They also considered more realistic model in which multi-quantum well structure of field-free QCL band structure was continued into the leads. In this case electrons enter/exit device with density of states that better mirrors density of states in the surrounding QCL periods. Wacker *et al.* [14] were able to find the solution of NEGF equations for "periodic" boundary condition imposed onto Green's functions. Their calculations, however, were not made in real space, which is the case considered here.

The number of iterations required to get self-consistent solution of NEGF equations depends on the scattering mechanism (functions Σ^R, $\Sigma^<$) included into the calculations. For dissipative transport the major role plays the scattering by the phonons. In this case Σs contain terms, which depend on $E \pm \hbar\omega$, where $\hbar\omega$ is the phonon energy. In one iteration step $G^{R,<}$ are perturbed at $E \pm \hbar\omega$, then. Thus, the number of iterations required for spreading the perturbation over the range of energies ΔE covered by the electrons in the structure must exceed $\mathrm{iter}_{min} = \Delta E/\hbar\omega$. The lower limit for ΔE can easily be estimated as $\Delta E > eU$, where U is the voltage applied to the structure. For GaAs-based QCLs, polar-optical phonon with $\hbar\omega \approx 36$ meV prevails, hence $\mathrm{iter}_{min} \approx 1.5$ for THz QCLs which are biased by $U \approx 50$ mV/per period [21], [22] and usually one period is used in the calculations. For mIR QCLs which operate under $U \approx 250$ mV/per period [23], [24] $\mathrm{iter}_{min} \approx 7$. In practice these numbers should be multiplied by the factor 3 to 4 to achieve satisfactory degree of consistency.

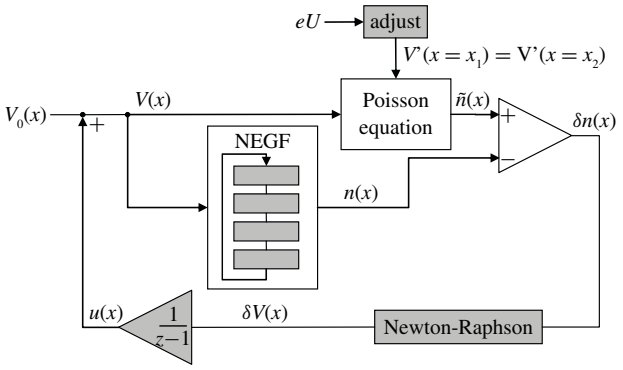

Fig. 1. Diagram of self-consistent NEGF-Poisson calculations used for THz QCL [10]–[12]. The integrator $1/(z-1)$ appears on the z-transform scheme because corrections δV_i are cumulated in successive iterations $u_i = u_{i-1} + \delta V_{i-1}$. $u(x)$ is the Hartree potential.

Further multiple increase in the number of iterations takes place when Poisson solver is incorporated into the formalism. Poisson equation is usually solved iteratively in the additional loop, outer with respect to the inner NEGF loop: self-consistent electron density $n(x)$ obtained at the output of NEGF simulator is used to calculate correction $\delta V(x)$ to the current potential which is sent back to the simulator input [25]. The scheme of iteration procedure is shown in the diagram of Fig. 1. Details of this diagram refer to the numerical Newton-Raphson method which enables one to calculate the correction $\delta V(x)$ upon the difference (error) $err(x) \equiv \delta n(x) P_c \equiv (\tilde{n}(x) - n(x))(edx)^2/\varepsilon$ between the density $n(x)$ and density $\tilde{n}(x)$ which is the solution of the Poisson equation

$$\frac{d}{dx}\varepsilon(x)\frac{dV(x)}{dx} = e^2\left[N_D(x) - \tilde{\mathrm{n}}(x)\right], \tag{4}$$

where $N_D(x)$ is the density of ionized dopants, and $\varepsilon(x) = \varepsilon_r(x)\varepsilon_0$ is dielectric constant. The correction δV changes the potential $V(x)$ in successive iterations until convergence i.e. $err(x) \cong 0$ is reached.

When modeling electronic devices an important issue is to preserve its electrical neutrality. Therefore (4) is solved with Neumann boundary conditions (constant field at the boundaries) applied to the potential at some $x = x_1$ and $x = x_2$. Then, the self-consistent solution $n(x) \cong \tilde{n}(x)$ assures charge neutrality

$$\rho \equiv \int_{x_1}^{x_2} dx\left(n\left(x\right) - N_D\left(x\right)\right) = 0.$$

The value of potential derivative $V'(x_1) = V'(x_2)$ is not unequivocally defined: it depends on the voltage applied to the structure, however its value is unknown. It must be adjusted until the current potential difference $eU_{\mathrm{cur}} = V(x_1) - V(x_2)$ becomes equal to the applied potential [11].

The whole computational scheme shown in Fig. 1 was successfully applied in [10]–[12], [18], [19] to the structure of resonant phonon THz QCL of [21]. The convergence of the numerical procedure was not discussed, but our simulations

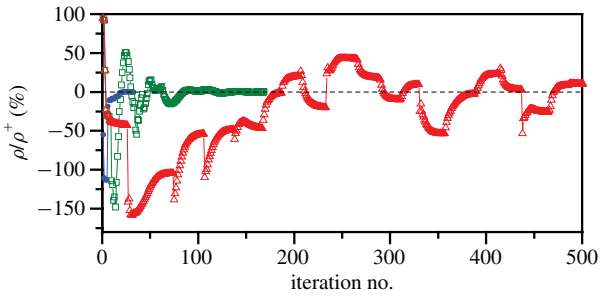

Fig. 2. Convergence of numerical procedures utilized in various NEGF/Poisson solvers: total charge ρ, in one laser period (in the units of ρ^+-charge of doping donors) versus the number of NEGF iterations. Series are for numerical scheme of Fig. 1 (•, Δ) or Fig. 3 (□) applied to 64 nm long structure of THz QCL of [21] (•), or 83 nm long structure of mIR QCL (Δ, □). In all cases homogeneous leads were attached to the structure and lesser contact selfenergies were calculated according to Fermi-Dirac distribution.

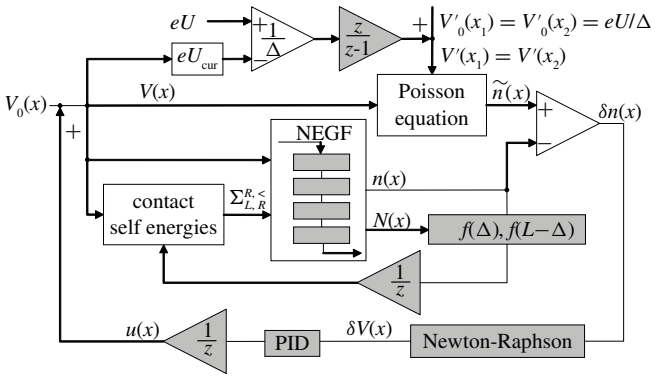

Fig. 3. z-transform flow chart of self-consistent solution of NEGF-Poisson equations used for mIR QCL. The signal at the output of PID block (controller) is the weighted sum of terms that are proportional to original (P) integrated (I) and differentiated (D) input signal (see (5)).

of such QCL show that 30–40 NEGF iterations are required to obtain the self-consistent solution of the equations which fulfills the convergence criteria (see Fig. 2). Hereafter these were assumed as less than 1% change in absolute values of the density of states $N(E, x)$ and the occupation function $f(E, x)$

$$|\delta N(E,x)| < 0.01, \quad |\delta f(E,x)| < 0.01,$$

and the value of error

$$|err(x)| < 2\mu eV$$

in each point x of the structure.

III. NEGF Modeling of mIR QCL

The procedure described in the previous section still works when applied to one period of mIR QCL strictly, although the number of iterations significantly increases. For the reasons to be explained in the next section, we also have made calculations for the structure consisting of more than one laser period. In such case Poisson equation must be solved with boundary conditions set *inside* the structure. Then, the numerical procedure that follows the diagram of Fig. 1 fails to converge. (see Fig. 2). In what follows, the development of computational scheme of Fig. 1, is described. It restores and considerably speeds up the convergence of the method and treats the leads attached to the structure of QCL subjected to NEGF calculations in a very realistic way.

A. Numerical Procedure

The changes we propose are summarized in the diagram of Fig. 3 and are as follows:

1) The outer "Poisson" loop is incorporated into the inner loop as the Hartree potential $u(x)$ is considered as additional real-valued self energy and treated as other self energies in NEGF formalism. ([20] p.307)
2) Poisson equation is solved only *inside* one laser period i.e. for $x_1 < x < x_2 = x_1 + \Delta$ with Neumann boundary conditions at x_1, x_2. This makes the laser period electrically neutral.

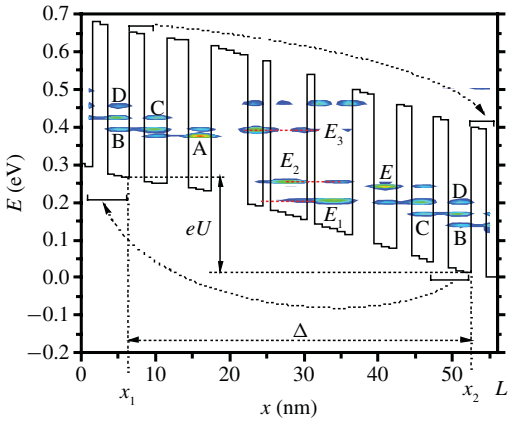

Fig. 4. Conduction band edge of mIR QCL structure used in the calculations (solid line). Laser period extends between $x_1 = 6$ nm and $x_2 = 52$ nm. Quantities and diagrams inside the figure illustrate numerical procedure 1–4 of Section III-A. Self-consistent solution of NEGF/Poisson equation is shown for $E_C(x)$ (solid line) and $1D$-density of states $N(E, k_{||}, x)$ for the vanishing in-plane momentum $k_{||}$ (color-filled plane).

3) The full NEGF formalism is applied to a bigger device of size $L > \Delta$ consisting of one laser period and parts of laser structure surrounding the period in question. As illustrated in Fig. 4, this can be done by copying $V(x_1 < x < x_2)$ with the energy shift of $\mp eU$ and the position (x) shift of $\pm\Delta$. Namely

$$V(0 \le x < x_1) = V(x + \Delta) + eU,$$
$$V(x_2 < x \le L) = V(x - \Delta) - eU.$$

Then, the relation $V(x + \Delta) = V(x) - eU$ holds for the whole device.
4) Dissipative multi-quantum well leads of [10] are attached to the device in the form of appropriate contact selfenergies. Unlike in [10] we introduce electric field into the leads: the potential inside the device is continued for one more laser period into the leads. Moreover, the occupation function which in (3) is used to calculate lesser contact selfenergies is a "periodic" repetition of *nonequilibrium* occupation function inside the device.

Namely,

$$f_L(E, k_{||}) = f(E - eU, k_{||}, x = \Delta),$$
$$f_R(E, k_{||}) = f(E + eU, k_{||}, x = L - \Delta).$$

Note that such self-consistent calculations of contact selfenergies are possible provided $L > \Delta$.[1]

5) Ideas from control theory were adopted to restore convergence of numerical procedure and make it more efficient. This issue will be described in detail in the next section.

B. Digital Controllers

Numerical procedures of Figs. 1 and 3 consist of the operations that are executed one after another. All the quantities, then, may be treated as the signals of discrete time, measured in the number of iterations. Therefore the diagrams in these figures contain z-transform operators acting on z-transformed signals. The diagrams contain feedback loops locking the object which is both nonlinear and inertial: the response $n(x)$ is nonlinear with the input $V(x)$, and delayed by $\tau \sim \Delta E/\hbar\omega$ as discussed in Sec. II. This could make the procedure unstable even if the object itself is stable. This may happen when too much correction in the wrong "phase" is sent back to the input, like in the diagram of Fig. 1, where the whole signal δV is integrated and feeds the input. Instead in the diagram of Fig. 3 the digital PID controllers are employed to precisely dose the amplitude and phase of the correction. For the main loop of Fig. 3 the Hartree correction in the i-th iteration is

$$u_i = K\left(\delta V_{i-1} + \frac{1}{T_I}\sum_{j=1}^{i-2}\delta V_j + T_D(\delta V_{i-1} + \delta V_{i-2})\right), \quad (5)$$

as compared to the correction

$$u_i = \sum_{j=1}^{i-1}\delta V_j,$$

being used in the diagram of Fig. 1. The latter is equivalent to purely I control of the object. As already mentioned, control like this could make the "dynamic system" defined by the structure of mIR QCL unstable. On the contrary, the PID control defined by (5) with appropriate values of the parameters K, T_I, T_D makes the system stable and enables one to find the response, which makes the error $err(x) \approx 0$ and the potential difference $eU_{\text{cur}} \approx eU$ with a desired precision.

The values of control parameters depend on the structure to be modeled and must be found experimentally. A good starting batch when searching for optimal values is $K \approx 2.5 \times \hbar\omega/\Delta E$ as for the proportionality factor and $T_I \approx 2$ for the integral constant. This pair has turned out most effective for the simulations of mIR QCL structure shown in Fig. 4. Details of these calculations and their results are described in the next section.

[1]Rules 2–4 relay mostly on the commonly-shared assumption about periodicity of quantum cascade structures. Discussion of nonperiodic effects which are supposed to exist in THz QCLs [10], [19], is beyond the scope of the paper. Therefore in the numerical example of Section III-C we use the bias $eU = 7\hbar\omega$ which anyway preserves electron density commensurable with geometrical period [10], [19].

C. Numerical Example

The structure of Fig. 4 refers to mIR QCL of Page *et al.* [23], who fabricated a device emitting IR radiation of $\lambda \approx 9$ μm for the threshold field of $F_{\text{th\_exp}} \approx 48$ kV/cm. Dimensions of real structure and that of Fig. 4 differ in that in our numerical model a real-space mesh of $dx = a = 1$ nm was assumed. So, wells and barriers real widths w_n were rounded to the nearest integers of w_n/a. With these round-offs the laser period was $\Delta = 46$ nm long and in the structure of Fig. 4 was located between the points $x_1 = 6$ nm and $x_2 = x_1 + \Delta = 52$ nm, which define the boundaries for the Poisson equation. Following rule 3 of Sec. III.A the whole structure used in NEGF calculations was larger: it contained two more barriers and extended between $x = 0$ and $x = L = 55$ nm. Contact selfenergies imitated leads described in rule 4 of Section III-A.[2]

Calculations were done for the temperature $T = 77$ K. The voltage applied to the laser period was $U = 0.252$ V, which corresponds to the average field of $F \approx 55$ kV/cm. The only scattering mechanisms included into NEGF formalism were LO-phonon scattering and interface roughness scattering. For the former the full off-diagonal character of this scattering was maintained [13]. For the latter exponential correlation function with the characteristic length of 4 nm and roughness height of 0.4 nm was assumed. We do not consider other scattering mechanisms as our aim is mainly to illustrate the numerical procedure described in the previous section. Moreover, it was shown recently that in case of mIR QCL incorporating merely those two is sufficient to reach excellent agreement between experimental and simulated data [26].

We completely solved the problem in $k_{||}$-space. Uniform sampling of total (E) and in-plane ($E_k \equiv \hbar^2 k_{||}^2/2m$) energy was used: the energy grid was $dE = dE_k = 6$ meV. Results of the calculations are summarized in Figs. 4–8. All quantities refer to self-consistent solution of NEGF/Poisson equations in which positional but not energy dependence of effective mass was taken into account.

The spectrum of all characteristic energies can be deduced from the inspection of 1D density of states for vanishing in-plane momentum $k_{||} = 0$. This is plotted in the form of 2D color-filled map in Fig. 4. Laser levels are denoted as E_1, E_2, and E_3. Injector levels are labeled A-E following the convention of [27]. An important issue to note is that leads we have implemented make the structure really periodic. In Fig. 4 the triplets of energy levels in the right/leftmost wells which belong to different QCL periods are shifted in energy scale exactly by eU. The occupation of these levels is also very similar as can be inferred from the inspection of the plots in Figs. 5 and 8, where the spectrum of current flowing through the structure is shown.

In general our calculations are consistent with current understanding of transport phenomena in this type of QCL. At the threshold current the upper laser level E_3 is fed from the injector levels A, B. The electrons leave the active region

[2]Following [10] the scattering time in the leads was $\tau_{sc} = 0.1$ ps. We have also performed calculations for $\tau_{sc} = 0.5$ ps and $\tau_{sc} = 0.05$ ps and found no major differences. E.g. total current through the structure has changed no more than by 5%.

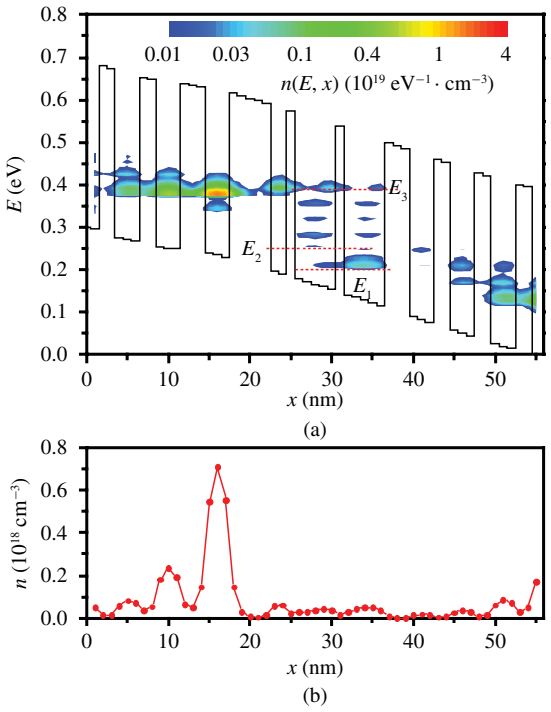

Fig. 5. (a) Energy-resolved electron density $n(E, x)$ (log-scaled color-map) versus conduction band edge $E_C(x)$ (line). (b) Electron density $n(x)$ in the structure of mIR QCL.

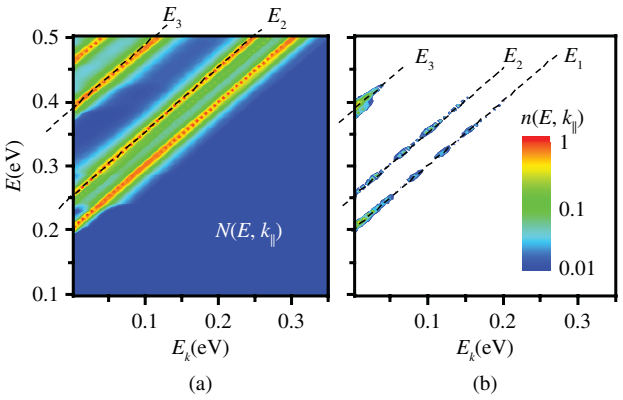

Fig. 6. Energy-momentum-resolved density of states $N(E, k_{||})$ (a) density of electrons $n(E, k_{||})$ (b) in the active region (23 nm< x <37 nm) of mIR QCL. All lines drawn in the figure are parallel: the distance between laser levels E_3 and E_2 decreases slightly with increasing $k_{||}$.

and enter injectors mainly by the direct tunneling from laser ground state E_1 into level D. As can be seen in Fig. 4 these levels lined up. The observed resonance delocalizes the involved wave functions and makes E_1-D transitions to carry the main streams of electrons leaving the active region. Note that similar E_1-D resonant coupling was found in MC simulations of [27].

In Fig. 5 electron densities are shown.

$$n(x) = \int_0^{\Delta E} dE n(E, x) = \int_0^{\Delta E} dE \int_0^{\sqrt{2mE}/\hbar} dk_{||} n\left(E, k_{||}, x\right).$$

The function $n(x)$ contains the charge integrated over all subbands so it cannot be used to find out whether or not the population inversion $\Delta n_{32} = n_3 - n_2$ exists in the laser. This information can be obtained from the inspection of the plot in Fig. 6(b) where the momentum-resolved density of electrons in the active region (AR) of QCL

$$n\left(E, k_{||}\right) = \int_{x \in \mathrm{AR}} dx n\left(E, k_{||}, x\right),$$

is shown as a map of (E, E_k)-variables. Distribution of electrons in the lower laser subband (E_2) and depopulating subband (E_1) follow a phonon-replica shape. In the upper laser subband the electrons are more thermalized and occupy only the states with low in-plane energy. Population inversion exists only for these states. On the contrary, for higher $k_{||}$-values the occupation of states is not inverted. As a result the global (all $k_{||}$) population inversion between laser subbands could not be reached. In such conditions, lasing is still possible what is confirmed by direct calculations of the material gain

$$g = -\frac{1}{\Delta} \int_{x_1}^{x_2} dx \alpha(h\nu, x),$$

where α is the absorption coefficient. Results of these calculations, performed according to the theory of [15] (terms with $\delta\Sigma$ omitted), are shown in Fig. 7. The main gain peak appears at $h\nu \approx 135$ meV. It is obvious that E_3–E_2 transition is responsible for this peak. However, also A-E_2 transition could give rise to the optical gain and form the peak at $h\nu =$ 120 meV in Fig. 7(b). Those two transitions are dominant in mid-infrared region [28]. Our calculations, then, show that A-E_2 transition typical for vertical QCLs [24] persist in diagonal structures in certain bias conditions. The maximal gain reaches the value of ≈ 70 cm^{-1} and slightly exceeds all optical losses divided by the confinement factor, which for the structure under consideration were estimated at 63 cm^{-1} [15]. Then, the value of F used in the calculations is our estimate of the threshold field: $F_{\mathrm{th\_cal}} \approx 55$ kV/cm which is not far from its experimental counterpart.

The location and width of the gain peak are also in agreement with experimental data. In the real structure lasing was found at the photon energy ≈ 131 meV, whereas electroluminescence spectra measured at 77 K typically have the full width at half maximum (FWHM) ≈ 12 meV [23]. Our estimate for the main gain peak in Fig. 7(b) also gives FWHM $\cong 2dE = 12$ meV.

From theoretical point of view, our "optical" results may cause some confusion, since it is known that lasing without global population inversion is possible only for nonparabolic subbands [29]-the phenomenon which was not incorporated in our calculations. It turns out however, that taking into account merely the positional dependence of effective mass is sufficient to explain the appearance of optical gain. In this case the barriers heights V_b in the quantum structure become $k_{||}$-dependent [3]

$$V_b(k_{||}) = V_b(k_{||} = 0) + \frac{\hbar^2 k_{||}^2}{2m_{\mathrm{well}}} \left(\frac{m_{\mathrm{well}}}{m_{\mathrm{barr}}} - 1\right)$$

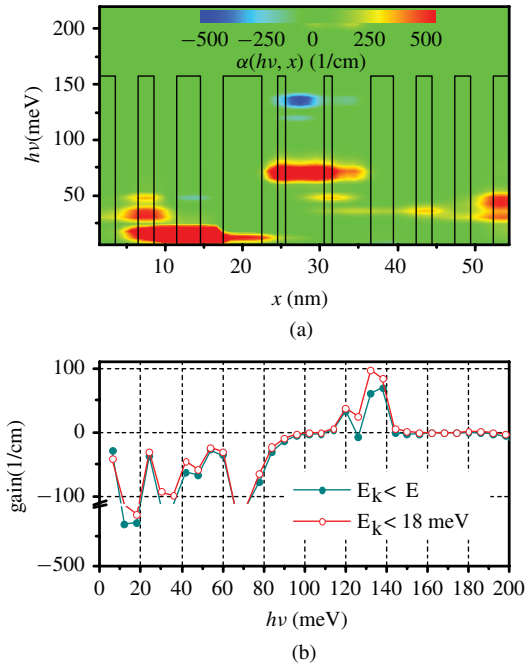

Fig. 7. (a) Spatially- and energy-resolved absorption coefficient $\alpha(h\nu, x)$. Color scale is provided only for $\alpha < 500$ cm^{-1}. Larger α are displayed in brown). QCL band structure (scale not provided) is shown to enable location of enhanced emission/absorption: lasing takes place in the first wide well of AR. (b) Total gain resulting from optical transitions between (•) all $k_{||}$ states (○) states with low in-plane energy: $E_k < 18$ meV.

and decrease with $k_{||}$ increasing because the term in the parenthesis is negative. Decrease of barrier height results in decrease of energy levels moreover the higher the level the larger its decrease. Consequently, the energy gap between subbands decreases with $k_{||}$ increasing. One could directly observe this effect in Fig. 6(a) where $k_{||}$-resolved density of states in the AR of QCL is shown. The gap $E_3 - E_2$ shrinks by some amount what prevents the absorption occurring at larger $k_{||}$-values destroying the gain. Instead, it rather gives rise to the negative peak that emerges directly on the low-frequency side of the gain peak. This scenario is also confirmed by direct calculation of the contribution to g resulting solely from the transitions between small-value $k_{||}$-states. Results of these calculations are shown in Fig. 7(b). Small-$k_{||}$-value transitions give the main contribution to g. Transitions between higher-value $k_{||}$-states suppress the gain only on its low-frequency part.

Spatially- and energy-resolved total current density $J(E, x)$ was calculated according to Eq. (20) in [3] and is shown in Fig. 8(a). It is worth mentioning that in our calculations current density $J(x)$ was conserved throughout the whole structure with the accuracy better than 0.5% which is known to be an important test of the correctness of NEGF calculations. For the applied field $F \approx F_{\text{th\_cal}}$ the total current density was $J \approx J_{\text{th\_cal}} \approx 4.2$ kA/cm^2. This value only slightly exceeds experimental value of the threshold current $J_{\text{th\_exp}} \approx 4$ kA/cm^2 [23]. Moreover, it appears that the whole I-V curve shown in Fig. 8(b) differs from the experimental one only in a scaling factor in electric field.

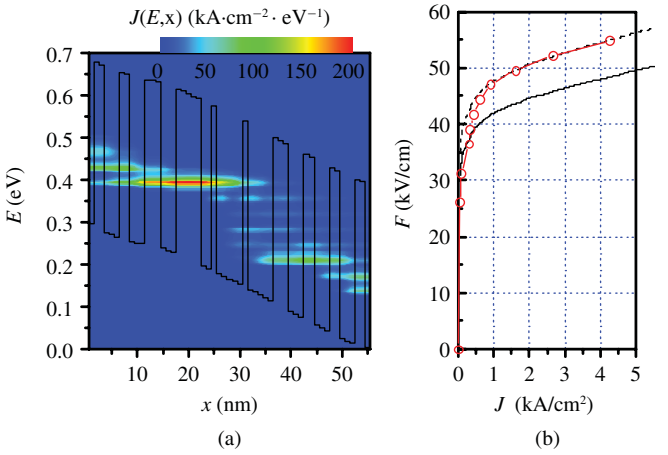

Fig. 8. (a) Spatially- and energy-resolved total current density $J(E, x)$ (color-filled plot) versus conduction band edge $E_C(x)$ of the structure. (b) Current-voltage characteristics of mIR QCL in the subthreshold region: (solid line) experimental [23] (dashed line) experimental scaled by the factor $F_{\text{th\_cal}}/F_{\text{th\_exp}}$ (○) calculated.

D. Discussion

In the previous section we were able to get results that fairly well agree with the experiment although some important physics i.e. nonparabolicity and e-e scattering were not implemented in the model. The former is known to lower eigenenergies and the distance between them. If not taken into account, it should result in larger photon energy $h\nu$. This was not observed because the effect was cancelled by the difference in the width of the layers in real and simulated structures. Namely, level E_3 went down as the real width 1.9 nm of first well in AR was rounded to 2 nm and simultaneously level E_2 went up as the real width 5.4 nm of second well in AR was rounded to 5 nm. This has helped to keep photon energy close to the experimental value but not the I-V curve. According to the theory of Kazarinov and Suris [30] the latter depends mostly on energy coupling ground state in the injector (A) with level E_3. The injecting barrier which proceeds AR has original width of 4.7 nm as compared to the value of 5 nm used in the model. Such increase makes the coupling energy lower. Then, the field required to reach some current density is larger in the model than in original structure. Therefore our estimate was $F_{\text{th\_cal}} > F_{\text{th\_exp}}$.

Concerning e-e scattering our results suggest that this mechanism is less important than LO-phonon and interface roughness scatterings (at least as for the quantities considered in this paper). To some extent our result is similar to that of [27], [31] where excellent agreement between theoretical and experimental characteristics of mIR QCL was found, although e-e scattering was not included in the model.

IV. Conclusion

To the best of our knowledge, NEGF calculations of mIR QCL that preserve real space basis, have never been performed. The approach developed in this paper keeps a real space basis and relies on two improvements introduced to NEGF/Poisson computational scheme. First, our contact self energies take into account electrical field in the leads and

nonequilibrium occupation function and thus better imitates periodicity of QCL structure. Second, NEGF/Poisson solver was equipped with several controlling features that restore the convergence of the method for complex quantum structures with boundary conditions for Poisson equation set inside devices. As an example, calculations for anticrossed diagonal design of QCL have been performed. Our results in general correspond to the current understanding of carrier transport in such devices. We believe that further conclusions will be possible when more systematic studies for different roughness scattering parameters, temperatures, QCL designs etc. are carried out. NEGF approach is known to be not only an alternative method for getting numerical solutions of the problems related to various transport phenomena, but also a method that provides access and deep insight into to the features inaccessible with other simulation tools.

ACKNOWLEDGMENT

The authors would like to thank T. Kubis for clarifying comments and helpful advice on nonequilibrium Green's function and his multiquantum-well leads and to M. Bugajski for useful discussions and comments on electronic transport in quantum cascade lasers.

REFERENCES

[1] L. V. Keldysh, "Diagram technique for non-equilibrium processes," *Sov. Phys. JETP*, vol. 20, no. 4, pp. 1018–1026, 1965.

[2] L. P. Kadanoff and G. Baym, *Quantum Statistical Mechanics: Green's Function Methods in Equilibrium and Non-Equilibrium Problems*. Redwood City, CA: Benjamin Cummings, 1995.

[3] R. Lake, G. Klimeck, R. C. Bowen, and D. Jovanovic, "Single and multiband modeling of quantum electron transport through layered semiconductor devices," *J. Appl. Phys.*, vol. 81, no. 12, pp. 7845–7869, Jun. 1997.

[4] R. C. Bowen, G. Klimeck, R. K. Lake, W. R. Frensley, and T. Moise, "Quantitative simulation of a resonant tunneling diode," *J. Appl. Phys.*, vol. 81, no. 7, pp. 3207–3213, Apr. 1997.

[5] J. Wang, E. Polizzi, and M. Lundstrom, "A 3-D quantum simulation of silicon nanowire transistors with the effective-mass approximation," *J. Appl. Phys.*, vol. 96, no. 4, pp. 2192–2203, Aug. 2004.

[6] M. Pourfath and H. Kosina, "Computational study of carbon-based electronics," *J. Comput. Electron.*, vol. 8, nos. 3–4, pp. 427–440, Oct. 2009.

[7] S. Steiger, R. G. Veprek, and B. Witzigmann, "Electroluminescence from a quantum-well LED using NEGF," in *Proc. 13th Int. Workshop Comput. Electron.*, Beijing, China, May 2009, pp. 1–4.

[8] L. E. Henrickson, "Nonequilibrium photocurrent modeling in resonant tunneling photodetectors," *J. Appl. Phys.*, vol. 91, no. 10, pp. 6273–6281, Mar. 2002.

[9] U. Aeberhard and R. H. Morf, "Microscopic nonequilibrium theory of quantum well solar cells," *Phys. Rev. B*, vol. 77, no. 12, pp. 125343-1–125343-10, Mar. 2008.

[10] T. Kubis, C. Yeh, and P. Vogl, "Theory of nonequilibrium quantum transport and energy dissipation in terahertz quantum cascade lasers," *Phys. Rev. B*, vol. 79, no. 19, pp. 195323-1–195323-10, May 2009.

[11] T. Kubis, C. Yeh, and P. Vogl, "Quantum theory of transport and optical gain in quantum cascade lasers," *Phys. Stat. Sol. (C)*, vol. 5, no. 1, pp. 232–235, Jan. 2008.

[12] T. Kubis, C. Yeh, and P. Vogl, "Non-equilibrium quantum transport theory: Current and gain in quantum cascade lasers," *J. Comput. Electron.*, vol. 7, no. 3, pp. 432–435, 2008.

[13] T. Kubis and P. Vogl, "Self-consistent quantum transport theory: Applications and assessment of approximate models," *J. Comput. Electron.*, vol. 6, nos. 1–3, pp. 183–186, 2007.

[14] S.-C. Lee and A. Wacker, "Nonequilibrium Green's function theory for transport and gain properties of quantum cascade structures," *Phys. Rev. B*, vol. 66, no. 24, pp. 245314-1–245314-18, 2002.

[15] A. Wacker, "GaIn in quantum cascade lasers and superlattices: A quantum transport theory," *Phys. Rev. B*, vol. 66, no. 8, pp. 085326-1–085326-7, 2002.

[16] A. Wacker and B. Y.-K. Hu, "Theory of transmission through disordered superlattices," *Phys. Rev. B*, vol. 60, no. 23, pp. 16039–16049, Dec. 1999.

[17] A. Wacker, "Coherence and spatial resolution of transport in quantum cascade lasers," *Phys. Stat. Sol. (C)*, vol. 5, no. 1, pp. 215–220, Jan. 2007.

[18] H. Callebaut, "Analysis of the electron transport properties in quantum cascade lasers," Ph.D. thesis, Dept. Electr. Eng. Comput. Sci., Massachusetts Inst. Technol., Cambridge, 2006.

[19] T. Kubis and P. Vogl, "How periodic are terahertz quantum cascade lasers?" *J. Phys.: Conf. Ser.*, vol. 193, no. 1, p. 012063, Nov. 2009.

[20] S. Datta, *Electronic Transport in Mesoscopic Systems*. Cambridge, U.K.: Cambridge Univ. Press, May 1997.

[21] A. Benz, G. Fasching, A. M. Andrews, M. Martl, K. Unterrainer, T. Roch, W. Schrenk, S. Golka, and G. Strasser, "Influence of doping on the performance of terahertz quantum-cascade lasers," *Appl. Phys. Lett.*, vol. 90, no. 10, pp. 101107-1–101107-3, May 2007.

[22] S. Kumar, B. S. Williams, S. Kohen, Q. Hu, and J. L. Reno, "Continuous-wave operation of terahertz quantum-cascade lasers above liquid-nitrogen temperature," *Appl. Phys. Lett.*, vol. 84, no. 14, pp. 2494–2496, Apr. 2004.

[23] H. Page, C. Becker, A. Robertson, G. Glastre, V. Ortiz, and C. Sirtori, "300 K operation of a GaAs-based quantum-cascade laser at $\lambda \approx 9\ \mu$m," *Appl. Phys. Lett.*, vol. 78, no. 22, pp. 3529–3531, May 2001.

[24] C. Sirtori, P. Kruck, S. Barbieri, P. Collot, J. Nagle, M. Beck, J. Faist, and U. Oesterle, "GaAs/Al_xGa_{1-x}As quantum cascade lasers," *Appl. Phys. Lett.*, vol. 73, no. 24, pp. 3486–3488, 1998.

[25] R. Lake and S. Datta, "Non equilibrium Green's-function method applied to double-barrier resonant-tunneling diodes," *Phys. Rev. B*, vol. 45, no. 12, pp. 6670–6685, Mar. 1992.

[26] A. Wittmann Y. Bonetti, J. Faist, E. Gini, and M. Giovannini, "Intersubband linewidths in quantum cascade laser designs," *Appl. Phys. Lett.*, vol. 93, no. 14, pp. 141103-1–141103-3, Oct. 2008.

[27] R. C. Iotti and F. Rossi, "Nature of charge transport in quantum-cascade lasers," *Phys. Rev. Lett.*, vol. 87, no. 14, pp. 146603-1–146603-4, Sep. 2001.

[28] M. F. Pereira, Jr., S.-C. Lee, and A. Wacker, "Controlling many-body effects in the midinfrared gain and terahertz absorption of quantum cascade laser structures," *Phys. Rev. B*, vol. 69, no. 20, pp. 205310-1–205310-7, May 2004.

[29] J. Faist, F. Capasso, C. Sirtori, D. L. Sivco, A. L. Hutchinson, M. S. Hybertsen, and A. Y. Cho, "Quantum cascade lasers without intersubband population inversion," *Phys. Rev. Lett.*, vol. 76, no. 3, pp. 411–414, Jan. 1996.

[30] R. F. Kazarinov and R. A. Suris, "Possibility of amplification of electromagnetic waves in a superconductor with a superlattice," *Fiz. Tekh. Poluprov.*, vol. 5, no. 4, pp. 797–800, 1971.

[31] A. Bismuto, R. Terazzi, M. Beck, and J. Faist, "Electrically tunable, high performance quantum cascade laser," *Appl. Phys. Lett.*, vol. 96, no. 14, pp. 141105-1–141105-3, Apr. 2010.

Grzegorz Hałdaś received the M.S. degree in electrical engineering from Rzeszow University of Technology (RUT), Rzeszow, Poland, in 1995, and the Ph.D. degree from the Institute of Electron Technology, Warsaw, Poland, in 2003.

He has been with the Department of Electronics Fundamentals at RUT since 1995. He is the author or co-author of more than 20 publications on electrical transport in mesoscopic systems. His current research interests include quantum cascade lasers, implementation of nonequilibrium Green's functions method, and transport in semiconductor nanostructures.

Andrzej Kolek received the M.Sc. degree from the Akademia Górniczo-Hutnicza University of Science and Technology, Krakow, Poland, in 1982, the Ph.D. degree from the Warsaw University of Technology, Warsaw, Poland, in 1990, and the D.Sc. degree from Wroclaw University of Technology, Wroclaw, Poland, in 1997, all in electronics.

He has been with the Department of Electronics Fundamentals, Rzeszow University of Technology (RUT), Rzeszow, Poland, since 1982, and is currently the Head of the Department. From 2002 to 2008, he was the Vice-Dean of the Faculty of Electrical and Computer Engineering at RUT. In 2007, he was a Professor of Technical Sciences. He has authored or co-authored over 50 research papers, published mostly in highly regarded international journals and conference proceedings. He is involved in theoretical and experimental studies on noise in electronic materials and devices. His current research interests include modeling of conduction in metal-insulator composites, percolation systems, and nanoelectronic devices.

Prof. Kolek is a member of the International Microelectronics and Packaging Society. In 2005, he joined the Section of Electronic Materials and Technologies of the Committee on Electronics and Telecommunication of the Polish Academy of Sciences, and the Polish Association of Theoretical and Applied Electrotechnics.

Igor Tralle received the M.S. degree in physics from the Belarusian State University, Minsk, Belarus, in 1971, the Ph.D. degree in physics from the Institute of Physics of the National Academy of Sciences of Belarus, Minsk, in 1981, and the D.Sc. degree in physics from the Belarusian State University in 1996.

He was a Visiting Researcher at the Electrical and Computer Engineering Department, Northwestern University, Evanston, IL, from 2001 to 2002. He is now the Head of the Mesoscopic and Statistical Physics Department, Institute of Physics, University of Rzeszow, Rzeszow, Poland. He is the author or co-author of more than 90 publications in prestigious scientific journals. His current research interests include semiconductor physics, physics of low-dimensional structures, spintronics, optoelectronics, and mathematical physics.